Universität Karlsruhe (TH)
Institut für Baustatik

FE–Modeling of Fiber Reinforced Polymer Structures

W. Wagner, F. Gruttmann

Mitteilung 7(2002)

Universität Karlsruhe (TH)
Institut für Baustatik

FE–Modeling of Fiber Reinforced Polymer Structures

W. Wagner, F. Gruttmann

Mitteilung 7(2002)

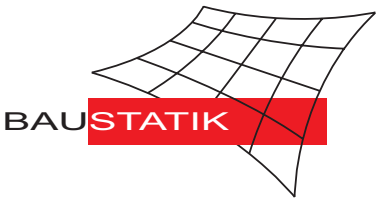

Prof. Dr.–Ing. W. Wagner
Institut für Baustatik
Universität Karlsruhe
Postfach 6980
76128 Karlsruhe

Telefon: (0721) 608–2280
Telefax: (0721) 608–6015
E–mail: bs@.uni-karlsruhe.de
Internet: http://www.bs.uni-karlsruhe.de

WCCM V
Fifth World Congress on
Computational Mechanics
July 7–12, 2002, Vienna, Austria
Eds.: H.A. Mang, F.G. Rammerstorfer,
J. Eberhardsteiner

FE–Modeling of Fiber Reinforced Polymer Structures

W. Wagner*

Institut für Baustatik
Universität Karlsruhe (TH), Kaiserstr. 12, D–76131 Karlsruhe, Germany
e-mail: ww@bs.uka.de

F. Gruttmann

Institut für Statik
Technische Universität Darmstadt, Alexanderstr. 7, D–64283 Darmstadt, Germany
e-mail: gruttmann@statik.tu-darmstadt.de

Key words: composite material, layered shell elements, hexahedral elements, delamination, stability algorithms

Abstract
Carbon fiber reinforced polymer materials are often used in light weighted thin–walled structures. In this paper we describe different finite element models for the nonlinear analysis of global and local effects in composite structures. Shell elements based on the first order shear deformation theory are able to describe the global behaviour sufficiently. Especially along free edges relatively large interlaminar stresses occur which may lead to local failure modes like delamination and in addition to local buckling of sublayers. Different approaches to consider these effects are discussed. In a first model the individual layers are discretized using hexahedral elements. Due to the applied EAS–method and ANS–method the elements can be used even for thin structures. Alternatively a shell-like 2D–modeling based on the introduction of a multi–director theory can be adopted. Additional degrees of freedom for each layer lead to a sufficient representation of the three–dimensional stress state. The delamination behaviour at layer boundaries is described using special interface elements. The efficiency, the advantages and the range of application of the different models are shown with several numerical examples, e.g. the stability behaviour of a composite panel and the delamination behaviour of a plate.

1 Introduction

Composite materials are often used in light weighted thin–walled structures. Besides the global structural behaviour frequently local damage effects, e.g. delamination have to be investigated. To study such problems the complicated 3D–stress state - especially in thickness direction - has to be evaluated. Here, in general a numerical calculation of the problem e.g. with finite elements is necessary. In this paper we discuss different finite element strategies to model thin composite structures. An overview is given in Fig. 1.

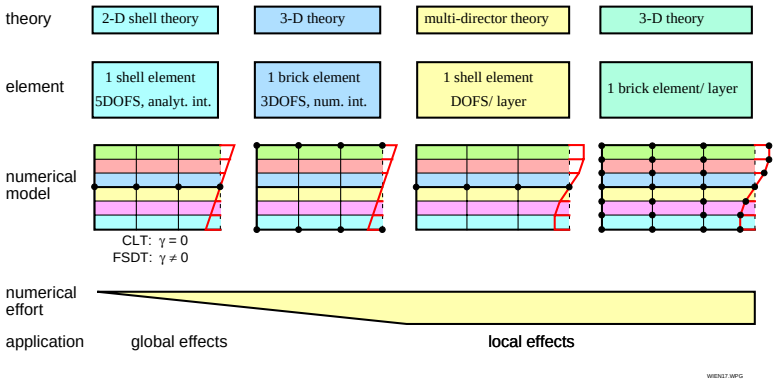

Figure 1: Finite element modeling of thin composite structures

Within a first approach shell elements based on the first order shear deformation theory with inextensible director vector are used. Usually the elements possess 5 nodal degrees of freedom, whereas elements with 6 or 7 nodal degrees of freedom are applied if intersections occur or if thickness changes have to be taken into account, respectively. These models are sufficient to describe the global behaviour of structures. Secondly 3D–brick elements with an appropriate thickness integration can be used (linear elements with enhancements or at least quadratic shape functions). The third alternative are brick–type shell elements where only displacements at the bottom and top surface of the shell are introduced, see e.g. Parisch [9]. The fourth method is the use of a shell-like 2D–modeling based on the introduction of a multi–director formulation, see e.g. [12], [4], [5]. Within this approach a director for each layer is introduced, which leads to an improved representation of the transverse shear stresses. If thickness changes for each layer are allowed, at least layerwise constant normal stresses in thickness direction can be described. Especially, 4-node elements have been successfully used. Finally, the fifth method is to use at least one brick element for each individual layer. Concerning 3D-modeling of stringer stiffened shell panels we refer also to e.g. [14], [16].

In this paper, an overview on the geometrical and physical nonlinear formulations is given. Some examples demonstrate the range of applicability of the different models.

2 Element formulations to describe the global behaviour

2.1 Elements based on the first order shear deformation theory

Elements based on the so–called first order shear deformation theory are quite standard. Concerning theoretical and numerical details for such formulations we refer to the literature. An overview is given in

the textbook [8]. A relatively simple formulation where finite rotations are taken into account is described in [17].

2.2 Formulations for hexahedral elements

Hexahedral elements based on standard displacement formulations exhibit a severe locking behaviour, especially if these elements are applied to thin structures. It is well known that the standard isoparametric eight–node element with trilinear shape functions can be essentially improved when applying the assumed strain method (ANS) to some strain components. Following [1] the transverse shear strains of the middle plane are independently interpolated using special shape functions. The thickness strains are approximated considering the approach in [2]. Furthermore, the membrane behaviour is improved by applying the enhanced assumed strain method (EAS) with five or more parameters [13]. A variational formulation and detailed finite element equations of an ANS–EAS5–element may be found in [7]. On the other hand an improved element behaviour can be achieved with tri–quadratic shape functions, but here on element level already 20 or 27 nodes are necessary.

In general these elements have to be used in such a way that one element is necessary for each layer. This may not be effective to analyze the global behaviour of the structure. In order to use only one element in thickness direction the layer sequence must be considered within the thickness integration. The evaluation of the stiffness matrix and residual load vector is performed using a numerical Gauss integration. For a hexahedral element with tri–linear shape functions two integration points are sufficient for each direction. Thus, in total eight integration points are used for each individual layer of the laminate. After the first isoparametric map, see Fig. 2, one can introduce a second isoparametric map for each layer.

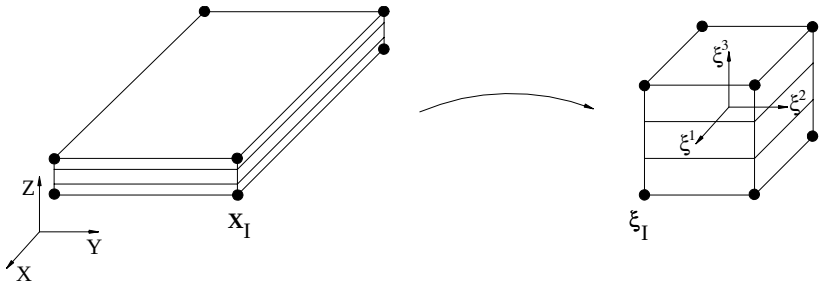

Figure 2: First isoparametric map for the element geometry

The local coordinates $\boldsymbol{\xi} = [\xi^1, \xi^2, \xi^3]^T$ are interpolated as

$$\boldsymbol{\xi} = \sum_{i=1}^{nlay} \bar{N}_i \;\; \boldsymbol{\xi}_i \;\; , \qquad \text{with} \qquad \bar{N}_i = \frac{1}{8}(1 + r^1 \, r_i^1)(1 + r^2 \, r_i^2)(1 + r^3 \, r_i^3) \, , \tag{1}$$

where i denotes the node number and $\boldsymbol{\xi}_i$ contains the coordinates of the considered layer. The coordinates $\mathbf{r} = [r^1, r^2, r^3]^T$, with $-1 \leq r^i \leq +1$ are defined with a second isoparametric space, see Fig. 3. To evaluate the element matrices one has to sum over all layers $nlay$ and over all integration points $ngaus$. As example, the integration of the element stiffness matrix $\mathbf{K}_{e\,IJ}$ of nodes I,J reads

$$\mathbf{K}_{e\,IJ} = \sum_{L=1}^{nlay} \sum_{igaus=1}^{ngaus} \left[\, \mathbf{B}_I^T(\boldsymbol{\xi}_{gp}^L) \, \mathbb{C}_L \, \mathbf{B}_J(\boldsymbol{\xi}_{gp}^L) + \mathbf{G}_{IJ}(\boldsymbol{\xi}_{gp}^L) \right] \; \det \mathbf{J}(\boldsymbol{\xi}_{gp}^L) \det \mathbf{J}^L(\mathbf{r}_{gp}^L) \, w_{gp}^L \, . \tag{2}$$

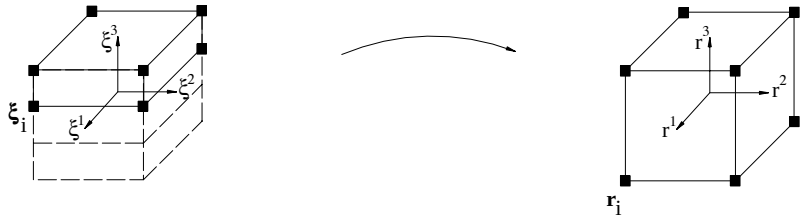

Figure 3: Second isoparametic map for the layer geometry

Here, $\mathbf{B}_I, \mathbf{B}_J$ and $\mathbf{G}_{IJ}$ describe the discrete strain–displacement relations and the geometrical matrix using a standard notation. The matrix $\mathbb{C}_L$ denotes the orthotropic material matrix and $\mathbf{J}$ and $\mathbf{J}^L$ the Jacobian matrix of the first and second map, respectively. Furthermore, w_{gp} are the weighting factors of the considered integration point.

3 Element formulations to describe local effects

An overview on possible local effects, especially effects which describe failure or damage, in composite material has been given in [8], see Fig. 4, or in [10].

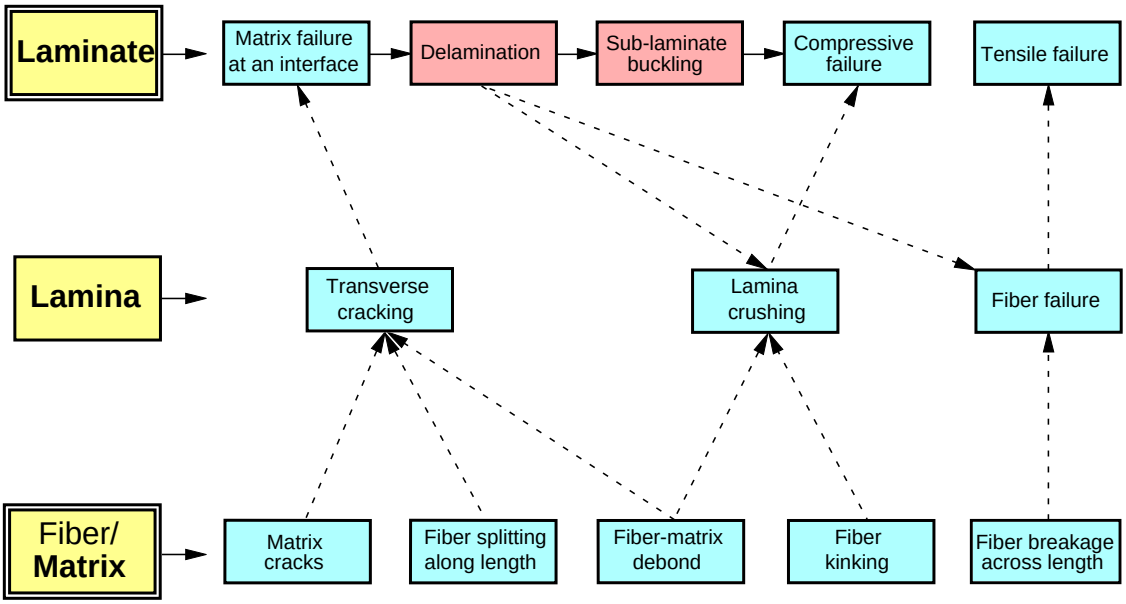

Figure 4: Failure modes in composite structures

At first we describe possible element formulations to calculate the complicated 3D-stress state. Here for example edge effects have to be mentioned. As the diagram shows there is a complicated interaction of the different failure modes. In this paper we focus on the delamination problem. The interaction of failure at the layer boundaries with the damage mechanism in the plies is not considered.

3.1 Hexahedral element formulations

The above described hexahedral element formulations can be used to describe local effects. Each layer is discretized using one element in thickness direction. Changes of thickness for each layer are possible and layerwise constant normal stresses in thickness direction can be described. Furthermore warping effects are incorporated.

3.2 Multi–director formulation

A multi–director formulation provides an alternative approach for a sufficient accurate evaluation of the interlaminar stresses. The numerical treatment requires only a two–dimensional discretization of the reference surface Ω, which can be seen as an essential advantage. The input of the complicated layer sequence for laminates is independent of the surface discretization. The n **physical** layers of thickness h^j of the laminate are described with N **numerical** layers of thickness h^i. Thus each physical layer can be subdivided into several sublayers or vice versa several layers can be summarized to an equivalent numerical layer.

The initial geometry is described by an arbitrary reference surface and a normal vector as in standard shell theories. Thus the position vector $\mathbf{X}_0$ of the reference surface is labeled with convective coordinates Θ^α. An orthonormal basis system $\mathbf{t}_k(\Theta^\alpha)$ is attached to this surface, where $\mathbf{t}_3$ is the normal vector and Θ^3 the coordinate in thickness direction $(h_u \leq \Theta^3 \leq h_o)$. The transformations between the different base systems are achieved using a proper orthogonal tensor $\mathbf{R}_0$

$$\mathbf{t}_k(\Theta^\alpha) = \mathbf{R}_0(\Theta^\alpha)\,\mathbf{e}_k\,. \tag{3}$$

Introducing a displacement field $\mathbf{u}(\Theta^i)$ the position vectors of the reference and the current configuration are given by

$$\begin{aligned} \mathbf{X}(\Theta^\alpha,\Theta^3) &= \mathbf{X}_0(\Theta^\alpha) + \Theta^3\,\mathbf{t}_3(\Theta^\alpha) \\ \mathbf{x}(\Theta^\alpha,\Theta^3) &= \mathbf{X}(\Theta^\alpha,\Theta^3) + \mathbf{u}(\Theta^\alpha,\Theta^3)\,. \end{aligned} \tag{4}$$

For the displacement field $\mathbf{u}(\Theta^i)$ in shell space we assume a multiplicative decomposition with independent functions for the shape in thickness direction and functions defined on the reference surface of the shell. The displacement vector of the numerical layer i is interpolated through the thickness by

$$\begin{aligned} \mathbf{u}(\Theta^\alpha,\Theta^3) &= \sum_{l=1}^{m} \phi_l^i(\Theta^3)\,\bar{\mathbf{u}}_l^i(\Theta^\alpha) = \mathbf{\Phi}^i(\Theta^3)\,\bar{\mathbf{u}}^i(\Theta^\alpha) \\ \bar{\mathbf{u}}^i(\Theta^\alpha) &= [\bar{\mathbf{u}}_1^i, \bar{\mathbf{u}}_2^i, \quad \ldots \quad, \bar{\mathbf{u}}_m^i]^T \quad (2 \leq m \leq 4)\,. \end{aligned} \tag{5}$$

The shape functions are arranged in a matrix

$$\mathbf{\Phi}^i = [\phi_1^i\mathbf{1}, \phi_2^i\mathbf{1}, \quad \ldots \quad, \phi_m^i\mathbf{1}] \tag{6}$$

with hierarchical functions ϕ_l^i up to third order. Thus eq. (5) allows warping of the cross sections and thickness change.

The 2. Piola-Kirchhoff stress tensor $\mathbf{S}$ and the work conjugated Green–Lagrange strain tensor $\mathbf{E}$ which appear in the principle of virtual work are formulated with respect to convected base vectors. For this purpose the covariant base vectors of the reference configuration are computed as $\mathbf{G}_i = \partial\mathbf{X}/\partial\Theta^i$ whereas

the dual base vectors $\mathbf{G}^i$ are defined by $\mathbf{G}_i \cdot \mathbf{G}^j = \delta_i{}^j$. Accordingly, one obtains the convected base vectors $\mathbf{g}_i$ and $\mathbf{g}^j$ of the current configuration. Each ply is considered as a homogeneous orthotropic medium, where the axes of orthotropy coincide with the material principal axes. Hence the stresses of the physical layer j are given by the material law $\mathbf{S} = \mathbf{C}\,\mathbf{E}$. Top and bottom surface of the shell are loaded, whereas body forces are neglected for simplicity.

An associated 4–node isoparametric shell element can be described straight forward. Shear locking is avoided adapting a procedure according to Bathe and Dvorkin [1]. Details are given in Refs. [4], [5].

3.3 Delamination model

A delamination model using interface layers has been described in [15],[18]. Here, only the basic ideas and assumptions are given. Fig. 5 shows a finite element discretization of a plate strip using eight–node elements. The interface layers, with thickness h_t, are positioned in those regions where delamination is expected. The numerical investigations showed that the behaviour of the global composite structure remains practically unaltered for thickness ratios of $h_t/h \leq 10^{-2}$, where h denotes the thickness of the total laminate, see Fig. 6. The delamination criterion of Hashin [6] in terms of the interlaminar normal

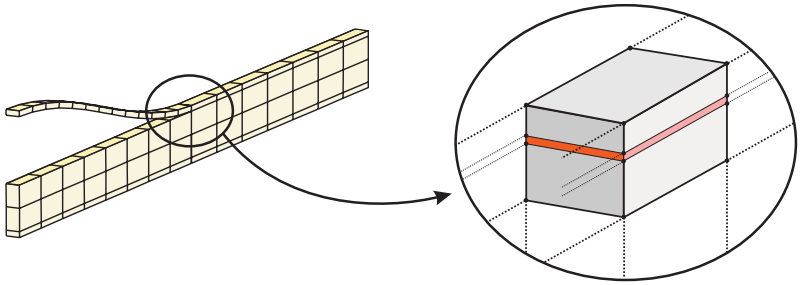

Figure 5: Plate strip with delaminated layer and interface element

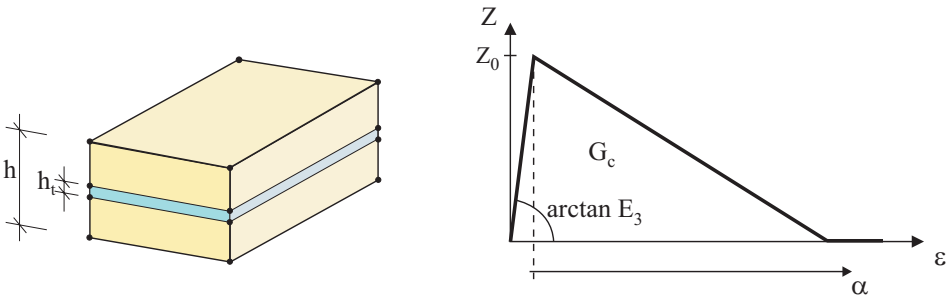

Figure 6: Interface layer and softening function

stresses S^{33} and shear stresses S^{13} and S^{23} is used to predict the location where delamination occurs. Introducing a local Cartesian coordinate system one obtains

$$\frac{(S^{33})^2}{Z_0^2} + \frac{(S^{13})^2 + (S^{23})^2}{R_0^2} \leq 1\,. \tag{7}$$

Here, Z_0 and R_0 denote the tensile strength in thickness direction and the shear strength of the laminate, respectively. The criterion can only be formulated in terms of Second Piola Kirchhoff stresses $\mathbf{S}$, if the

application is restricted to small deformations. Otherwise the transformation to the Cauchy stress tensor $\boldsymbol{\sigma}$ has to be considered. A graphical interpretation of this criterion is given in Fig. 7.

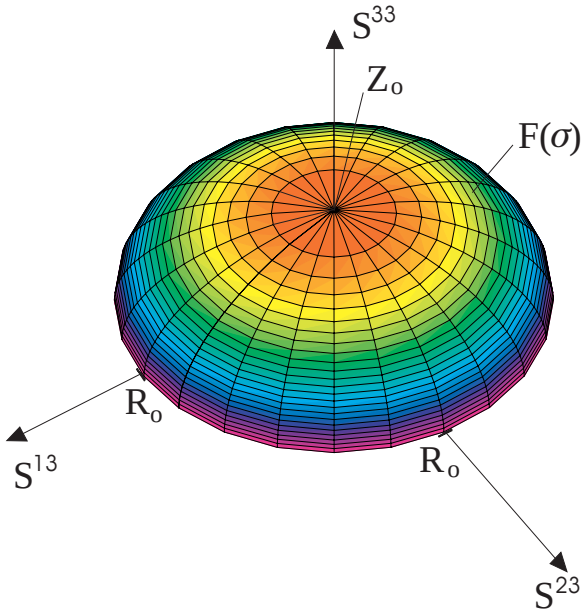

Figure 7: Hashin criterion

Furthermore, linear softening behaviour according to Fig. 6 is introduced

$$Z(\alpha) = Z_0\,(1 - \mu\alpha) \geq 0 \qquad \text{with} \quad \mu > 0\,, \tag{8}$$

where the internal variable α denotes the equivalent inelastic strain. The critical energy release G_c rate corresponds to the area under the softening curve. Considering that the energy is dissipated in the interface layer of thickness h_t one obtains

$$G_c = \frac{Z_0^2 h_t}{2}\,(\frac{1}{E_3} + \frac{1}{Z_0\mu})\,, \tag{9}$$

where E_3 denotes the elastic modulus in thickness direction. If the elastic deformations are negligible, which means that the first term in the sum cancels out, the softening parameter μ can easily be determined from (9) as

$$\mu \;=\; \frac{Z_0\;h_t}{2\;G_c}\,. \tag{10}$$

Delamination is defined, when the absolute value of the interlaminar stress vector vanishes. Details of the associated viscoplastic material model and the numerical implementation are described in [15],[18].

4 Examples for global effects

4.1 Clamped cylindrical shell panel

The nonlinear behaviour of a clamped cylindrical shell panel of composite material under a uniform load for a cross ply $[0^o, 90^o]$ has been analyzed in [11] using a finite element model based on the von Kármán equations. Geometrical and material data are:

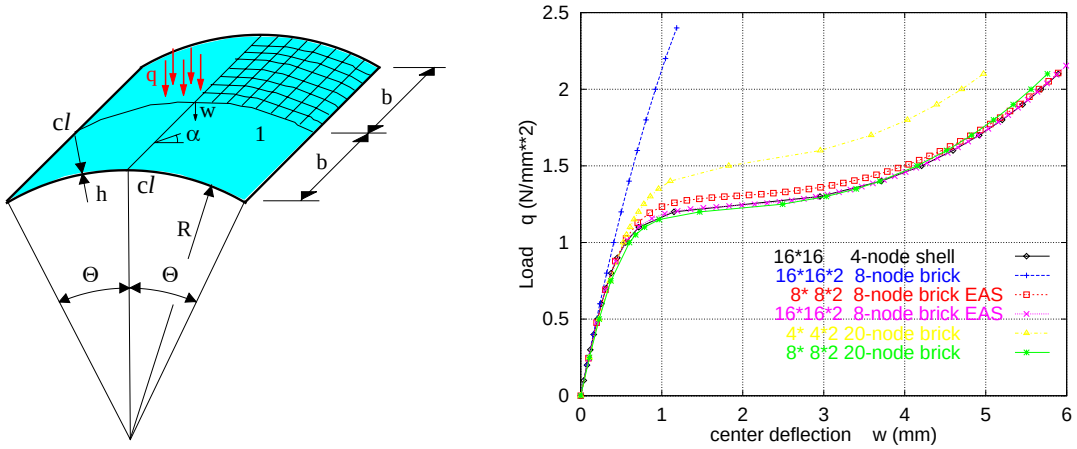

Figure 8: Load deflection curves for a shell panel under uniform load

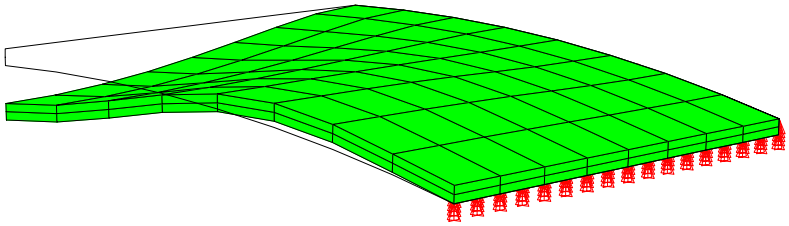

Figure 9: Deformed mesh for a shell panel under uniform load (zscale=3, uscale=2)

$$
\begin{array}{llllllllll}
R & = & 2540 & in\,, & E_{11} & = & 25\cdot 10^6 & psi\,, & G_{12} & = & 0.5\cdot 10^6 & psi\,, \\
b & = & 254 & in\,, & E_{22} & = & 1\cdot 10^6 & psi\,, & G_{13} & = & 0.5\cdot 10^6 & psi\,, \\
h & = & 2.54 & in\,, & \nu & = & 0.25\,, & & G_{23} & = & 0.2\cdot 10^6 & psi\,, \\
\Theta & = & 0.1 & rad\,. & & & & & & & &
\end{array}
$$

We use this example to compare the results of different element formulations. The load deflection curves for the uniform load versus the center deflection are depicted in Fig. 8 using 8 x 8 and 16 x 16 finite element meshes for one quarter of the shell. Furthermore a deformed mesh is depicted in Fig. 9.

Due to the boundary conditions (clamped along the edges) a certain number of elements is necessary to give accurate results, especially in the range where large changes in the center displacement at nearly constant external loads occur. Excellent agreement in the results between shell elements and 3D–elements can be found over the whole range of deformation.

4.2 Buckling of a composite panel

Next we investigate the buckling behaviour of a cylindrical carbon fiber reinforced composite panel. Associated experiments with different thickness parameters for the skin have been carried out within an ESA contract by the Institute of Structural Mechanics of the ”Deutsches Zentrum für Luft- und Raumfahrt” (DLR) in Braunschweig, FRG. The panel consists of a cylinder segment with a radius of the middle surface $R = 370.9\ mm$ and six stiffeners, which are glued at the inner side of the skin, see Fig. 10. The skin

consists of 8 layers with a total thickness $H = 1\,mm$. The layer sequence is $[90°; \pm 45°; 0°]_{sym}$, where zero degree refers to the axial direction of the cylinder segment. The layer thickness is $h = 0.125\,mm$. The cross–section of a stiffener and its simplification in the numerical simulation is depicted in Fig. 11.

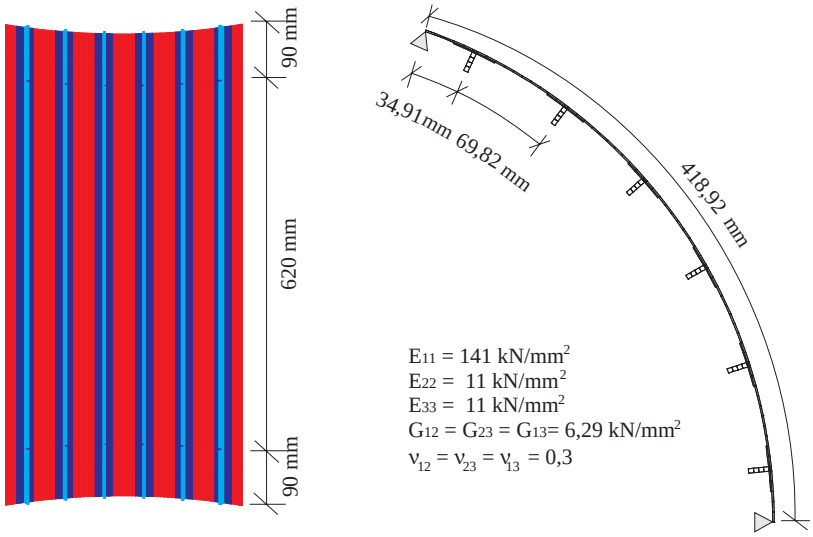

Figure 10: Geometry and material data; rear view and top view of the panel

The blade and the flange consist of 24 layers and 12 to 2 layers, respectively. Details of the layer sequence of the stiffener can be seen in Fig. 11. The layup of the skin and stiffener is symmetric. The finite

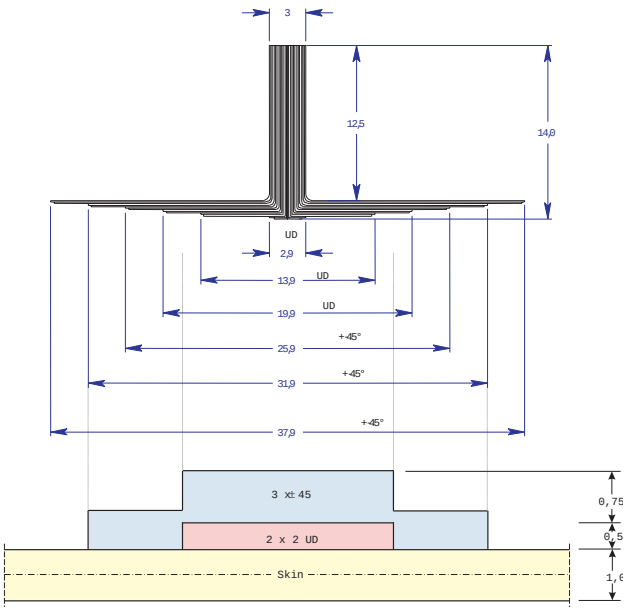

Figure 11: Cross–section of stiffener and its numerical model

element discretization with standard shell–elements is depicted in Fig. 12. The panel is discretized with 42 elements in length direction (40 elements for the inner range and 2 elements for the clamped range)

and 48 elements in circumferential direction. In total 3 meshes have been investigated, see Table 1.

Mesh	nodes	elements	dofs	buckling load [kN]
1	851	660	3407	151
2	2623	2268	12591	132
3	4171	3780	21087	118
Experiment				121

Table 1: Data of introduced FE–meshes and associated buckling loads

Furthermore, the radial displacements at the straight edges are set to zero. The boundary conditions are

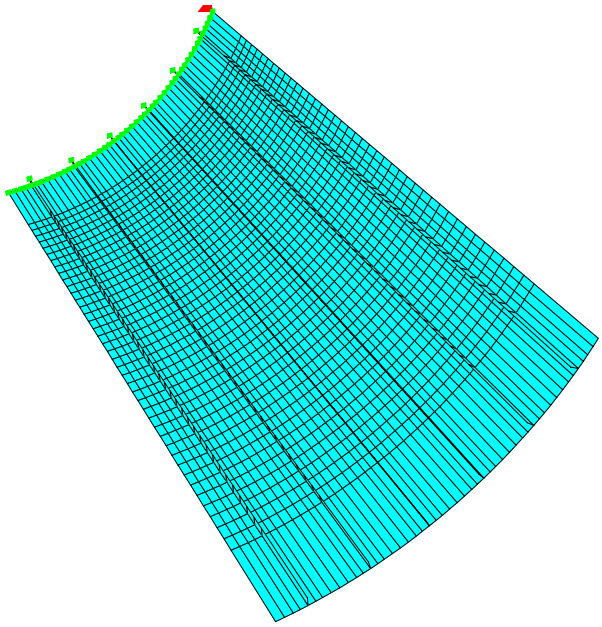

Figure 12: FE-mesh 2 of cylindrical panel

taken from the experiments and set as follows. The panel is clamped within a length of $90\,mm$ at both ends of the skin, where deflection in axial direction is possible. At the lower edge the panel is supported in axial direction. The panel is compressed at the top in axial direction. The results of the numerical investigations based on a linear elastic model are depicted in Fig. 13. As can be seen, the load deflection behaviour obtained with all finite element models is practically linear. The associated buckling loads are depicted in Table 1. The associated first and fifth eigenvectors of mesh 2 are shown in Fig. 15. The plots show local and global buckling modes of the skin. One should note, that the eigenvalues lie very close together. Thus, a small variation of any geometrical parameter or of the finite element model may change the shape of the eigenvectors. This holds especially when imperfections are taken into account. The stability behaviour of the panel is fairly sensitive with respect to geometrical imperfections of the skin. However due to missing data, this is not considered within the present finite element discretization. The agreement between the numerical results and the experimental results especially the buckling load is good. Similar results with a 3D–element have been reported in [7]. The deviations in the upper range of

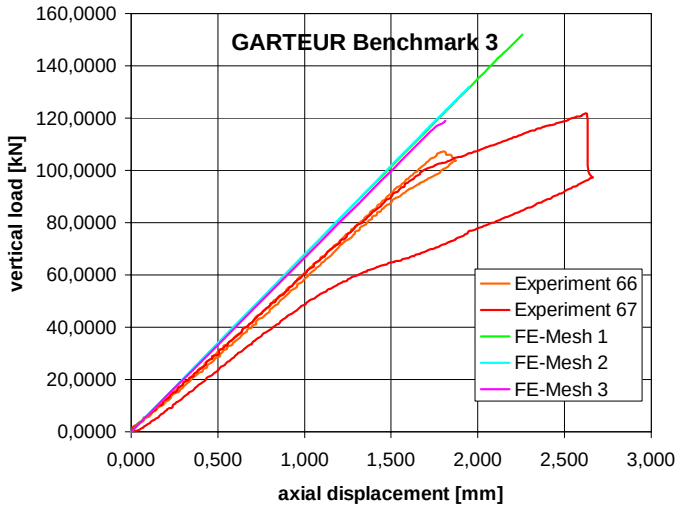

Figure 13: Load versus axial deflection of cylindrical panel

the load deflection curve follow from cracking effects between skin and stringers which are not contained in the present finite element model. Finally Fig. 16 shows the panel in the experimental buckling state.

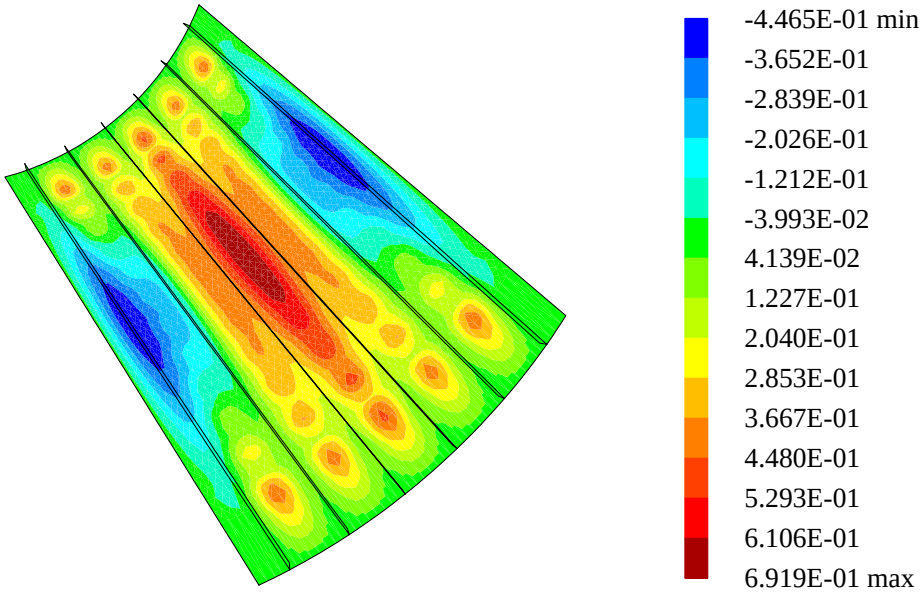

Figure 14: Radial displacements of cylindrical panel

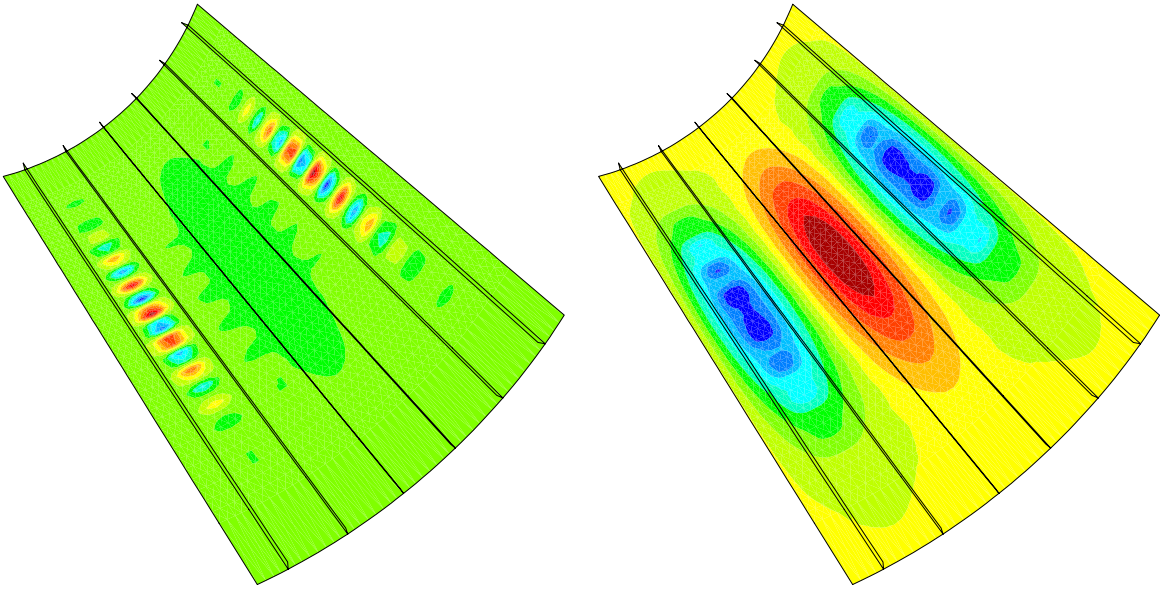

Figure 15: Radial components of the first and fifth eigenvector

Figure 16: Experimental buckling state of the carbon fiber reinforced panel (from DLR)

5 Examples for local effects

5.1 Layered plate subjected to uniform extension

In Figure 17 a rectangular plate under uniform extension is depicted. The laminate consists of four plies symmetrically stacked in $[0°/90°/90°/0°]$ stacking sequences where $0°$ refers to the x–direction. The width to height ratio is $b/h = 20$, where $h = 1\ mm$ represents one layer thickness and b half–width of the plate.

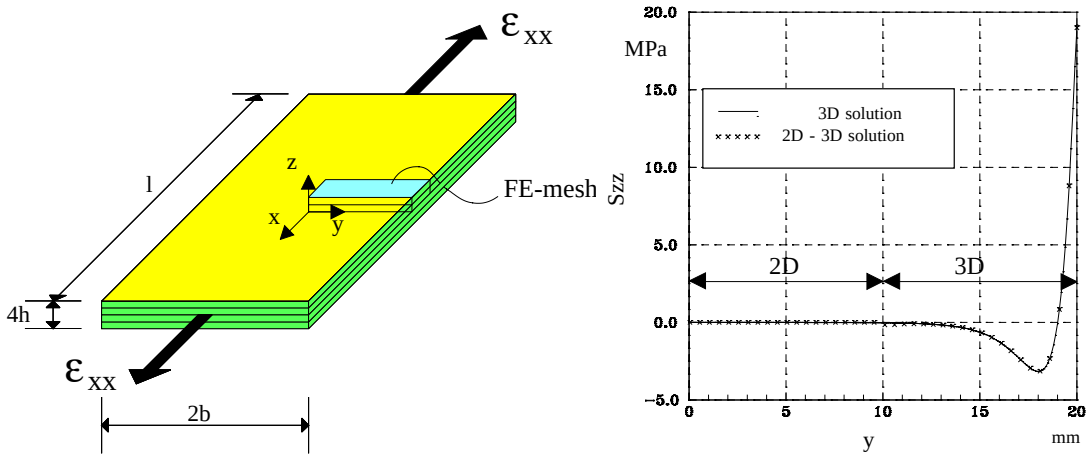

Figure 17: Rectangular plate subjected to uniform extension

The elastic constants with respect to principal material axes are:

$$\begin{aligned} E_{11} &= 137900 \quad MPa\,, & G_{12} &= 5860 \quad MPa\,, \\ E_{22} &= 14480 \quad MPa\,, & G_{23} &= 5860 \quad MPa\,, \\ \nu &= 0.25\,. \end{aligned}$$

Since the strain state is constant in x–direction, only one element is sufficient in this direction. Considering symmetry half the system is modeled with 70, 90, 110 elements and 8 layers in z–direction. The computation is carried out displacement controlled by prescribing u_x. In Figure 17 the stresses S_{zz} are plotted along the y–coordinate. The 3D solution is obtained with the above presented multi–director element [4], whereas the 2D solution is computed with standard 5–parameter shell elements. The plot shows that there is good agreement of the coupled 2D–3D solution with the 3D solution. The coupling element between 2D and 3D–models is described in [5]. The typical edge effect with relatively large edge stresses may lead to delamination.

5.2 Plate with initial circular delamination

The next example is a plate consisting of 16 layers with layer thickness $h_L = 0.12\,mm$ and stacking sequence $[0°/0°/+45°/0°/0°/-45°/0°/90°]_S$. A circular delamination is given between layer 14 and 15, see Fig. 18. Cochelin et.al.[3] investigated the stability behaviour of this structure with nongrowing delaminations. The plate is simply supported along the edges. The geometrical data and the material data

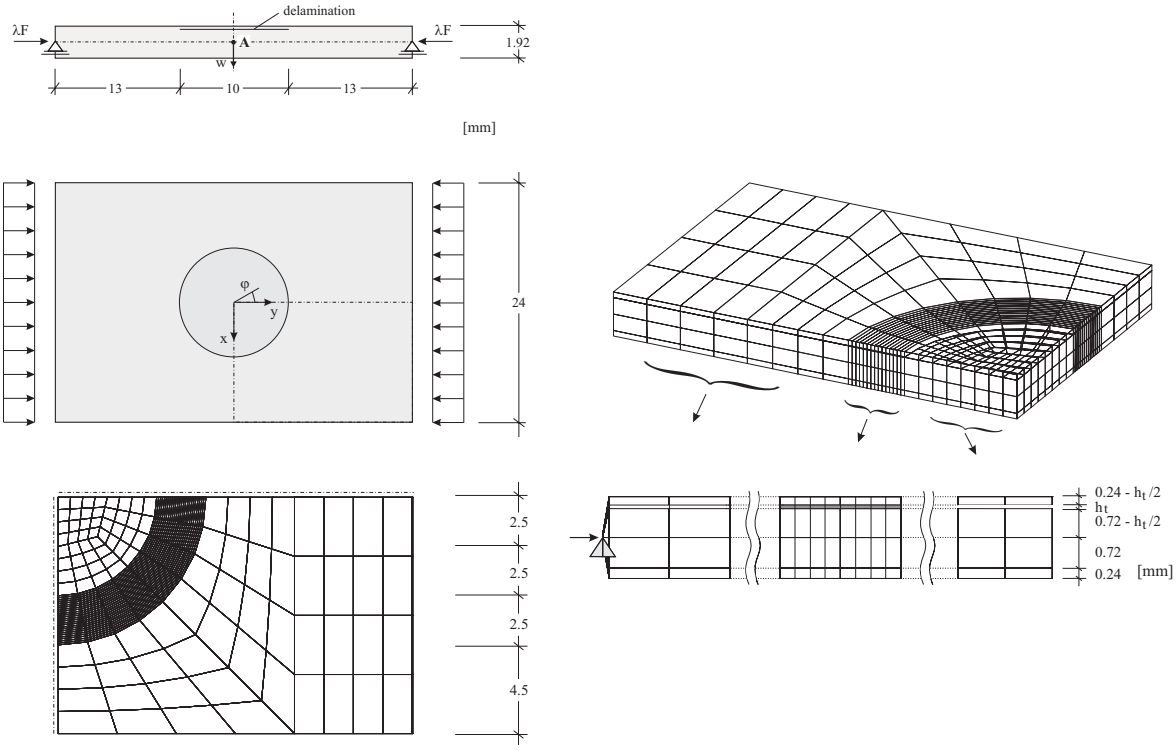

Figure 18: Plate with circular delamination: geometry and finite element mesh

for an AS/3501 graphite epoxy composite are given as follows:

$$
\begin{aligned}
E_{11} &= 135000 \;\; N/mm^2\,, & G_{12} &= 5150 \;\; N/mm^2\,,\\
E_{22} &= 8500 \;\; N/mm^2\,, & G_{23} &= 5150 \;\; N/mm^2\,,\\
\nu_{12} &= 0.317\,, & & \\
Z_0 &= 51.7 \;\; N/mm^2\,, & R_0 &= 91.0 \;\; N/mm^2\,,\\
h_t &= 0.005 \;\; mm\,, & F &= 30 \;\; N/mm\,.
\end{aligned}
$$

Due to the fibre angles with $\pm 45^\circ$ the structure is not symmetric with respect to the x–axis and y–axis, respectively. To reduce the computing effort this fact is ignored in the present analysis. The problem of propagating delaminations can in principle be studied when discretizing only one quarter of the plate using 3D–elements, see Fig. 18. Interface elements are positioned between the layers 14 and 15 only in the fine discretized annular space. In thickness direction several physical layers are summarized within one element layer. This has to be considered when performing the numerical integration in thickness direction. The nonlinear calculations are performed controlling the load parameter λ. First, we analyze a ”perfect” plate without delamination and thus without the interface layer. Due to the symmetric layup the plate is loaded as a pure membrane. With increasing axial deformation a bifurcation point is found. A switch to the secondary solution path is possible by a perturbation with the first eigenvector. Next, we analyze the behaviour of the plate with artificial and non growing delamination. In this case one obtains a load displacement curve which for large displacements approaches the secondary solution path of the perfect plate. Furthermore the solutions with increasing delamination zone are depicted in Fig. 19. The influence of time step Δt is negligible. Delamination starts at the coordinates $(x = 0\,mm, y = 5\,mm)$ and propagates along the inner circle. The whole process is depicted in Fig. 20.

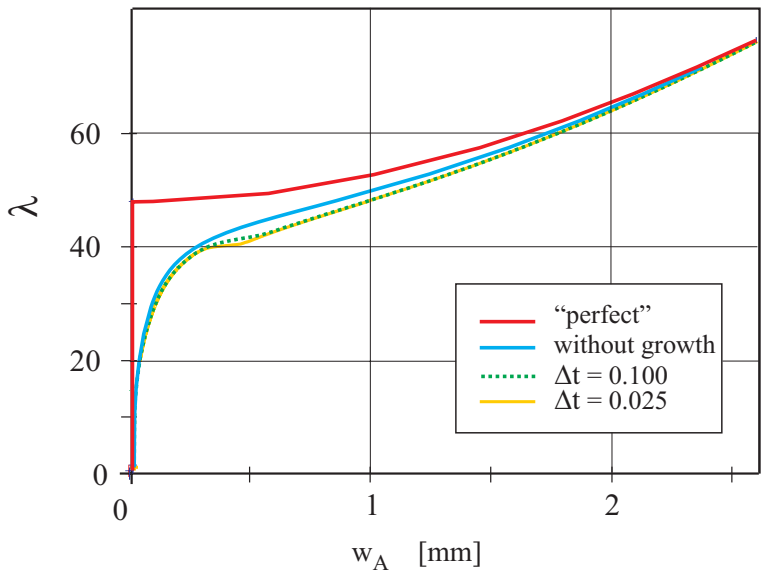

Figure 19: Load deflection curves of the plate

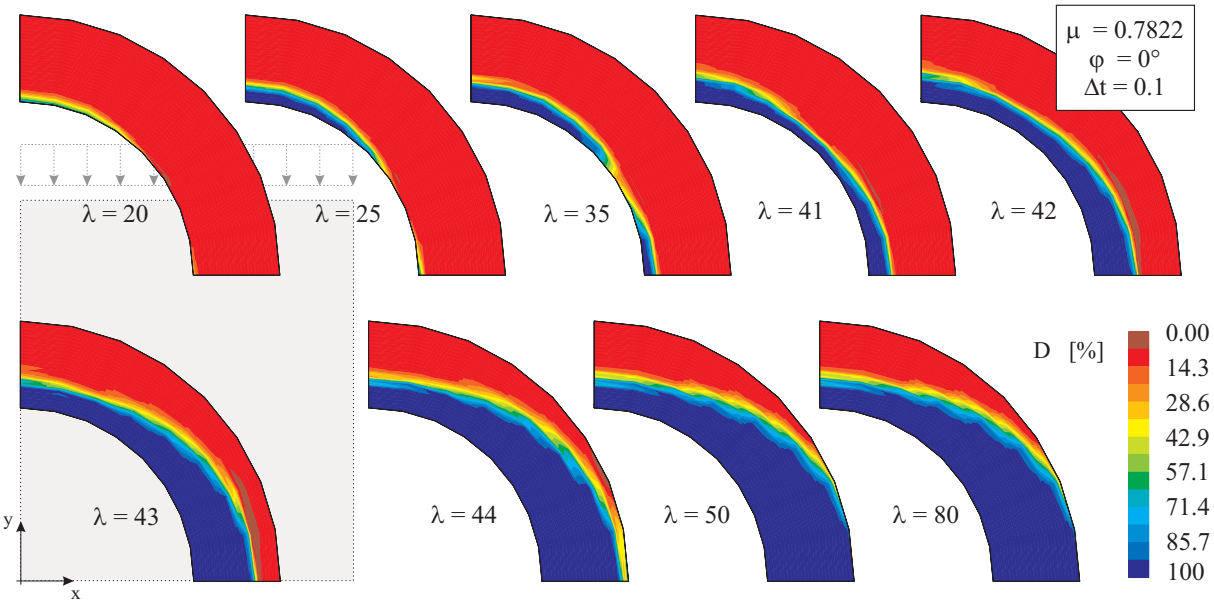

Figure 20: Growing delamination zone of the plate

6 Conclusions

In this paper we have described different finite element models for the nonlinear analysis of global and local effects in composite structures. Here, special shell elements and 3D-elements have been presented to describe global as well as local behaviour, which is dominated by a complicated 3D–stress state. The delamination problem has been solved using special interface elements. The efficiency, the advantages and the range of application of these models have been shown within several numerical examples.

Acknowledgements

Parts of this work have been funded by the Deutsche Forschungsgemeinschaft (DFG) which is gratefully acknowledged. Furthermore some of the numerical results of section 4.2 have been calculated in the Garteur Action Group 25 'Postbuckling and Collapse Analysis'.

References

[1] K. J. Bathe, E. Dvorkin, *A Continuum Mechanics Based Four Node Shell Element for General Nonlinear Analysis*, Engineering Computations, 1 (1984), 77–88.

[2] P. Betsch, E. Stein, *An Assumed Strain Approach Avoiding Artificial Thickness Straining for a Nonlinear 4-Node Shell Element*, Communications in Numerical Methods in Engineering, 11 (1995), 899–910.

[3] B. Cochelin, N. Damil, M. Potier-Ferry, *Asymptotic-Numerical Methods and Padé Approximants for Nonlinear-Elastic Structures*, Int. J. Num. Meth. Engng., 37, (1994), 1137–1213.

[4] F. Gruttmann, W. Wagner, *On the Numerical Analysis of Local Effects in Composite Structures*, Composite Structures, 29, (1994), 1–12.

[5] F. Gruttmann, W. Wagner, *Coupling of 2D– and 3D–Composite Shell Elements in Linear and Nonlinear Applications*, Comp. Meth. Appl. Mech. Eng., 129, (1996), 271–287.

[6] Z. Hashin, *Failure Criteria for Unidirectional Composites*, J. Appl. Mech., 47, (1980), 329–334.

[7] S. Klinkel, F. Gruttmann, W. Wagner, *A continuum based 3D–shell element for laminated structures*, Computers & Structures, 71, (1999), 43–62.

[8] O. O. Ochoa, J. N. Reddy, *Finite Element Analysis of Composite Laminates*, Kluwer Academic Publishers, Dordrecht/Boston/London (1992).

[9] H. Parisch, *A Continuum–Based Shell Theory for non–linear Applications*, Int. J. Num. Meth. Eng., 38, (1995), 1855–1883.

[10] F. G. Rammerstorfer, H. J. Böhm, *Finite Element Methods in Micromechanics of Composites and Foam Materials*, in B. H. V. Topping, ed., *Computational Mechanics for the Twenty-First Century*, Saxe-Coburg Publications, Edinburgh (2000), pp. 145-164.

[11] J. N. Reddy, K. Chandrashekhara, *Nonlinear Analysis of Laminated Shells including Transverse Shear Strains*, AIAA Journal, 23, (1985), 440–441.

[12] D. H. Robbins, J. N. Reddy, *Modeling of thick composites using a layer–wise laminate theory*, Int. J. Num. Meth. Eng., 36, (1993), 655–677.

[13] J. C. Simo, M. S. Rifai, *A Class of Mixed Assumed Strain Methods and the Method of Incompatible Modes*, Int. J. Num. Meth. Engng., 29 (1990), 1595–1638.

[14] I. C. Skrna-Jakl, M. A. Stiftinger, F. G. Rammerstorfer, *Numerical Investigations of an Imperfect Stringer-Stiffened Wing Torsion Box - An Analysis Concept*, Composites, 27B, (1996) 59-69.

[15] W. Sprenger, F. Gruttmann, W. Wagner, *Delamination growth analysis in laminated structures with continuum based 3D-shell elements and a viscoplastic softening model*, Computer Methods in Applied Mechanics and Engineering, 185, (2000), 123–139.

[16] M. A. Stiftinger, I. C. Skrna-Jakl, F. G. Rammerstorfer, *Buckling and Postbuckling Investigation of Imperfect Stringer-Stiffened Curved Composite Shells; Part B: Computational Investigations*, Thin-Walled Struct. 23, (1995) 339-350, 1995

[17] W. Wagner, F. Gruttmann, *A Simple Finite Rotation Formulation for Composite Shell Elements*, Engineering Computations, 11, (1994), 145–176.

[18] W. Wagner, F. Gruttmann, W. Sprenger, *A Finite Element Formulation for the Simulation of Propagating Delaminations in Layered Composite Structures*, Int. J. Num. Meth. Engng., 51, (2001), 1337–1359.